



Phase relations in the system Fe–Ni–Si to 200 GPa and 3900 K and implications for Earth's core

Tetsuya Komabayashi^{a,*}, Giacomo Pesce^a, Ryosuke Sinmyo^{b,1}, Takaaki Kawazoe^c, Helene Breton^a, Yuta Shimoyama^d, Konstantin Glazyrin^e, Zuzana Konôpková^e, Mohamed Mezouar^f

^a School of GeoSciences and Centre for Science at Extreme Conditions, University of Edinburgh, EH9 3FE, UK

^b Bayerisches Geoinstitut, Universität Bayreuth, 95440 Bayreuth, Germany

^c Department of Earth and Planetary Systems Science, Hiroshima University, Hiroshima, Japan

^d Department of Earth and Space Science, Osaka University, Osaka, Japan

^e Deutsches Elektronen-Synchrotron (DESY), Photon Science, Notekstrasse 85, 22607 Hamburg, Germany

^f European Synchrotron Radiation Facility, BP 220, F-38043 Grenoble Cedex, France

ARTICLE INFO

Article history:

Received 1 December 2018

Received in revised form 27 January 2019

Accepted 31 January 2019

Available online xxxx

Editor: J. Brodholt

Keywords:

Earth's core

high-pressure

diamond anvil cell

internal resistive heating

Fe–Ni–Si alloy

ABSTRACT

Phase relations in Fe–5 wt%Ni–4 wt%Si alloy was examined in an internally resistive heated diamond anvil cell under high pressure (P) and temperature (T) conditions to about 200 GPa and 3900 K by *in-situ* synchrotron X-ray diffraction. The hexagonal close-packed (hcp) structure was observed to the highest P – T condition, supporting the idea that the stable iron alloy structure in Earth's inner core is hcp. The P – T locations of the phase transition between the face-centred cubic (fcc) and hcp structures were also constrained to 106 GPa. The transition occurs at 15 GPa and 1000 K similar to for pure Fe. The Clausius–Clapeyron slope is however, 0.0480 GPa/K which is larger than reported slopes for Fe (0.0394 GPa/K), Fe–9.7 wt%Ni (0.0426 GPa/K), and Fe–4 wt%Si (0.0394 GPa/K), stabilising the fcc structure towards high pressure. Thus the simultaneous addition of Ni and Si to Fe increases the dP/dT slope of the fcc–hcp transition. This is associated with a small volume change upon transition in Fe–Ni–Si. The triple point, where the fcc, hcp, and liquid phases coexist in Fe–5 wt%Ni–4 wt%Si is placed at 145 GPa and 3750 K. The resulting melting temperature of the hcp phase at the inner core–outer core boundary lies at 550 K lower than in pure Fe.

© 2019 The Authors. Published by Elsevier B.V. This is an open access article under the CC BY-NC-ND license (<http://creativecommons.org/licenses/by-nc-nd/4.0/>).

1. Introduction

The density of Earth's core based on the seismological determination is likely lower than that of pure iron. Such a density deficit has been associated with the presence of light element(s) (Birch, 1952; Poirier, 1994; Allègre et al., 1995), which should have been incorporated in the core during core formation (Wade and Wood, 2005; Rubie et al., 2011; Siebert et al., 2013). The core density deficit (cdd) has been repeatedly revised from experimental measurements of iron density and recent estimates range from 3.6 to 4.6% for the solid inner core at 6000 K (Dewaele et al., 2006; Fei et al., 2016).

Silicon is considered a plausible candidate as the light element in the core as a consequence of metal–silicate equilibration during core formation process (Wade and Wood, 2005; Kawazoe and Ohtani, 2006; Georg et al., 2007; Fitoussi et al., 2009; Rubie et al., 2011; Shahar et al., 2011; Siebert et al., 2013; Hin et al., 2014). The system Fe–Si was extensively studied by experiment and theory (Alfè et al., 2002; Dobson et al., 2002; Lin et al., 2002; Kuwayama and Hirose, 2004; Lin et al., 2009; Fischer et al., 2013; Tateno et al., 2015; Ozawa et al., 2016). However, the system Fe–Ni–Si was less studied (Antonangeli et al., 2010; Sakai et al., 2011; Zhang et al., 2018; Morrison et al., 2018) although the core likely includes 5–10 wt% Ni from cosmochemical observations (McDonough, 2003). Sakai et al. (2011) examined the phase relations of Fe–4.8 wt%Ni–4.0 wt%Si (hereafter Fe–4.8Ni–4Si) in a laser-heated diamond anvil cell (DAC) with *in-situ* X-ray diffraction (XRD) and reported the stability of the hexagonal close-packed (hcp) structure to 304 GPa and 2780 K.

* Corresponding author.

E-mail address: tetsuya.komabayashi@ed.ac.uk (T. Komabayashi).

¹ Now at Department of Earth and Planetary Science, University of Tokyo, 7-3-1 Hongo, Bunkyo, Tokyo 113-0033, Japan.

On the other hand, Sakai et al. (2011) did not place constraints on a transition between the face-centred cubic (fcc) and hcp structures, although this is an important phase relation in the Fe alloys (Uchida et al., 2001; Asanuma et al., 2008; Komabayashi et al., 2009). Experimental investigations on the fcc–hcp transitions in Fe alloys revealed that the addition of Ni reduces the transition temperature (Mao et al., 2006; Komabayashi et al., 2012) whereas the Si incorporation has the opposite effect (Tateno et al., 2015; Komabayashi et al., 2019). From these observations, one can expect that the simultaneous addition of Ni and Si will not greatly move the boundary from the case of pure Fe, namely the effects of Ni and Si would cancel out. In this study, we report that the boundary in Fe–Ni–Si cannot readily be explained by a simple combination of the binary systems of Fe–Ni and Fe–Si.

We examined phase relations in Fe–Ni–Si alloy in an internally resistive heated DAC. The internal heating system produces high temperatures in the sample by its resistance. Thanks to the electric resistive heating, the accuracy in temperature is much improved with respect to the conventional laser heating (Komabayashi et al., 2009, 2012, 2019). Based on these experimental results, we will discuss the effect of simultaneous inclusion of Ni and Si on the Fe properties including the c/a ratio under high pressure (P)–temperature (T) condition and propose a new phase diagram for Fe–Ni–Si Earth's core.

2. Experimental procedure

High- P – T in-situ XRD experiments on an Fe–Ni–Si alloy sample were performed at the beamline P02.2 (ECB), PETRA III, DESY. X-rays with a wavelength of about 0.29 Å were focused to a $2 \times 2 \mu\text{m}^2$ spot at sample position and the diffracted X-rays were collected on a two dimensional detector (Perkin–Elmer XRD 1621). Similar experiments were also made at the beamline ID27, European Synchrotron Radiation Facility (ESRF) with X-rays with a wavelength of 0.3738 Å focused to a $3 \times 3 \mu\text{m}^2$ spot. At both beamlines, the collection time was 10 s for each XRD measurement. The obtained data were converted to the conventional one-dimensional XRD pattern using the fit-2D program (Hammersley, 1996).

High pressure was generated in a DAC with a pair of diamond anvils with a culet size of 300, 150, 120, or 90 μm bevelled depending on the pressure range. The starting material was a 5–7 μm thick Fe–5 wt%Ni–4 wt%Si alloy (hereafter Fe–5Ni–4Si, Rare Metallic Co.). Silica (SiO_2) glass layers served as a pressure transmitting medium and thermal insulator. High temperature was achieved with an internal resistive system (Komabayashi et al., 2009, 2012, 2019; Antonangeli et al., 2012). The sample was resistively heated by directly applying a DC voltage. Temperatures were measured by a spectral radiometric system with the optic system used in the laser heating experiment. The typical uncertainties in temperature were about 50 K (Komabayashi et al., 2012). Complementary laser heating experiments were also conducted on the same material at both P02.2 and ID27. See Liermann et al. (2010) and Morard et al. (2011) for details of the laser heating setup at each beamline.

Generated pressures in all the runs were calculated with a thermal equation of state (EoS) for the sample with the hcp structure. When the unit-cell volume for the hcp phase was not obtained, due to either grain growth or complete transition to the fcc phase, we assumed constant pressure upon further heating. The EoS was evaluated from the three systems with the hcp structure: Fe, Fe–Ni, and Fe–Si. The 300 K parameters for the Vinet EoS for Fe–5Ni–4Si were obtained by averaging on the basis of mole fraction between the three component systems. We assessed two sets of EoS parameters. Model A is based on pure iron (Dewaele et al., 2006), Fe–9.7 wt%Ni (Fe–9.7Ni, Komabayashi et al., 2012), and Fe–9 wt%Si (Fe–9Si, Tateno et al., 2015): $V_0 = 22.58 \text{ Å}^3$, $K_0 = 165 \text{ GPa}$, and $K' = 5.4$, where V_0 , K_0 , K' are the unit-cell volume, bulk mod-

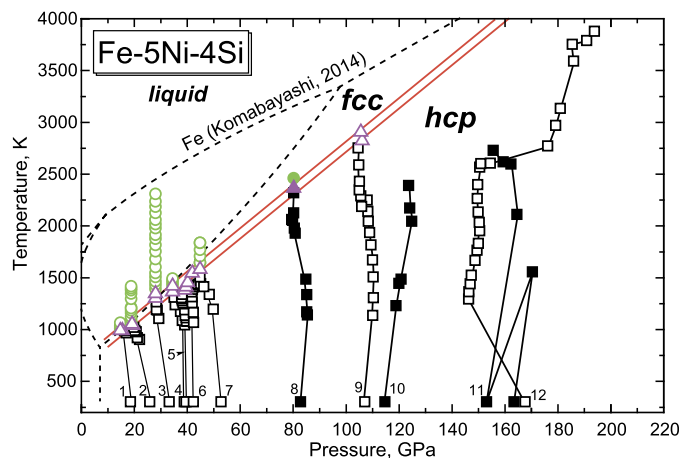


Fig. 1. Results of the experiments in Fe–5Ni–4Si. The phases observed in XRD patterns are plotted: square, hcp; triangle, fcc + hcp; circle, fcc. The open symbols are in the internally resistive heated DAC and solid symbols are in the laser-heated DAC. The phase relations in pure Fe were also plotted (Komabayashi, 2014). (For interpretation of the colours in the figure(s), the reader is referred to the web version of this article.)

ulus, and its pressure derivative at 300 K and 1 bar, respectively. We assumed the same thermal pressure terms as for pure iron (Dewaele et al., 2006; Tateno et al., 2015; Komabayashi et al., 2019). Very recently, Morrison et al. (2018) reported a compression study of Fe–11 wt%Ni–5.3 wt%Si (Fe–11Ni–5.3Si) and Fe–9.4 wt%Ni (Fe–9.4Ni) alloys with the hcp structure. We also created an EoS for our sample composition based on their parameters (Model B): $V_0 = 22.900(72) \text{ Å}^3$, $K_0 = 129.1(4.6) \text{ GPa}$, and $K' = 6.25(12)$. Compression curves for Model B and Morrison et al. (2018) are shown in Fig. S1 and they are nearly identical due to the close compositions, and therefore, we assumed the same (i) thermal pressure terms and (ii) uncertainty for each parameter as for Fe–11Ni–5.3Si (Morrison et al., 2018). All the parameters used are listed in Table 1. As will be discussed later, we choose Model B as our primary pressure scale and comparison of Models A and B would provide a reasonable uncertainty in the EoS for our sample.

3. Results

3.1. Phase relations in Fe–5Ni–4Si

Nine separate sets of in-situ XRD experiments were performed on the Fe–5Ni–4Si sample in the internally heated DAC and three in the laser-heated DAC. The results are summarized in Fig. 1 and Table S1. Note that the experimental pressures are based on the Model B EoS for the hcp sample. In all the runs we first compressed the sample to desired pressures and then started heating by resistance of the sample or laser.

The internal heating runs 1–4, and 7 and laser heating run 8 observed a transition sequence from the hcp to fcc structures with increasing temperature. In the first run, the sample was compressed to 19 GPa and the XRD pattern shows peaks from the hcp phase only. Then the sample was heated to 990 K and we observed coexistence of the hcp and fcc phases. The hcp phase disappeared at 1010 K. As the reversal reaction from the fcc towards hcp phase is very sluggish in binary systems (Komabayashi et al., 2012, 2019), we did not attempt to reverse it. In the 2 to 4th runs as well as the 1st run, we observed the transition sequence, hcp \rightarrow hcp + fcc \rightarrow fcc, with increasing temperature. Fig. 2 shows a series of XRD patterns collected near the transition during the 4th run for increasing temperature at 39 GPa. At 1310 K we observed the hcp phase only. Then we increased the temperature to 1360 K and the fcc (200) peak appeared. Further temperature increase to 1420 K completed the transition. As such the transition interval is less than 110 K.

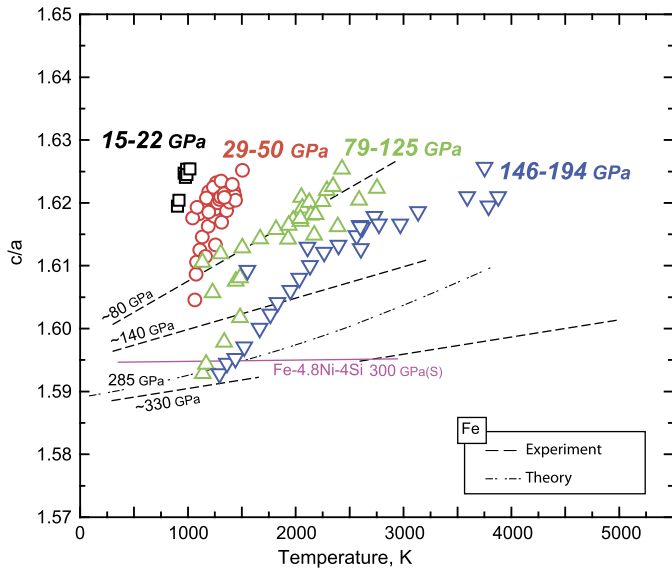


Fig. 4. The c/a ratio of the hcp phase (this study in Fe-5Ni-4Si; Sakai et al. (2011) in Fe-4.8Ni-4Si). Data for pure Fe are also plotted: experiment (Boehler et al., 2008; Tateno et al., 2010) and theory (Gannarelli et al., 2005).

sets of the EoS parameters of the hcp phase in the system Fe-Ni-Si (Table 1). Both EoS were modelled assuming a linear averaging scheme based on the mole fraction in the ternary system. As mentioned above, Model B is used as the primary EoS in this study since it is based on the established EoS for Fe-11Ni-5.3Si (Morrison et al., 2018) which is close to our sample composition. Indeed such a small compositional difference little affects the EoS parameters as evidenced by the fact that the compression curve of Model B is almost identical to that of Morrison et al. (2018) (Fig. S1). As such the experimental pressures in this study were reasonably constrained.

We also calculated the pressures based on another EoS (Model A) for consistency with existing works on the fcc-hcp transition boundary in Fe (Komabayashi et al., 2009), Fe-Ni (Komabayashi et al., 2012), and Fe-Si (Komabayashi et al., 2019), all of which employed the internal heating system in a DAC. The pressure scale used in each of those studies was based on the parameters for each component in Model A (Table 1).

Both Models A and B produce similar parameters for Fe-Ni hcp phases (Table 1) and therefore the major source for the difference in K_0 and K' for our Fe-Ni-Si hcp phase lies in the effect of Si in each Model. For Model A, Tateno et al. (2015) demonstrated that the addition of Si to hcp Fe increases the bulk modulus. For Model B, Morrison et al. (2018) showed that the addition of Si reduced K_0 and instead increased K' for Fe-Ni alloy with the hcp structure (Table 1). Nevertheless, the compression curves in Fig. S1 are similar between Models A and B, which results in the similar P - T conditions of the experiments, while Model B produced the fcc-hcp boundary with a little gentler dP/dT slope than Model A (Fig. 5).

The K_0 and K' values for the hcp phase with our sample composition are 165 GPa and 5.4 (Model A) and 129 GPa and 6.25 (Model B) respectively. These are comparable with the reported range for Fe-9Si hcp phase from 111 GPa and 6.08 to 168 GPa and 5.5 (Fischer et al., 2014; Tateno et al., 2015; Kamada et al., 2018). We take the comparison of Models A and B as a reasonable uncertainty range for the EoS of our sample. We will further discuss the uncertainty in the P - T conditions of the phase relations below, namely the triple point and phase relations to the inner core conditions.

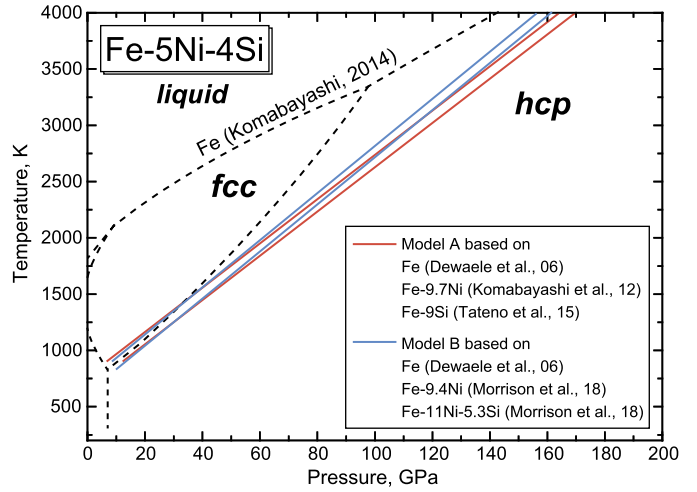


Fig. 5. Comparison of two EoS for the hcp structure to calculate experimental pressures. The fcc-hcp transition boundaries are plotted based on Models A and B EoS.

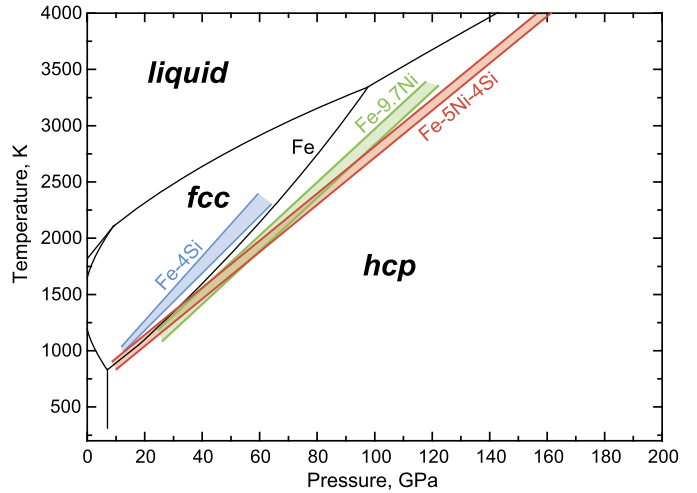


Fig. 6. Comparison of the fcc-hcp transition boundaries in four different compositions: Fe (Komabayashi et al., 2009; Komabayashi, 2014), Fe-9.7Ni (Komabayashi et al., 2012), Fe-4Si (Komabayashi et al., 2019), and Fe-5Ni-4Si (this study).

4.2. Effect of Si and Ni on the fcc-hcp transition

The present experiments placed constraints on the P - T locations of the fcc-hcp transition boundaries in Fe-5Ni-4Si (Fig. 1). Here we compare this result with existing data for pure Fe (Komabayashi et al., 2009) and the binary systems Fe-Ni (Komabayashi et al., 2012) and Fe-Si (Komabayashi et al., 2019). Note that all the fcc-hcp transitions in those four different systems were examined by the internally heated DAC, which enables us to make a precise comparison below.

Fig. 6 summarises the fcc-hcp transitions in those systems. The addition of Ni to Fe decreases the transition temperature (Mao et al., 2006; Komabayashi et al., 2012) whereas the transition temperature in the system Fe-Si is greater than in pure Fe (Tateno et al., 2015; Komabayashi et al., 2019). As such one may expect that the simultaneous addition of Ni and Si to Fe would cancel out their effects on the boundary location. Indeed, the present experiments below 30 GPa showed that the transition in Fe-5Ni-4Si took place at similar temperatures to the case in Fe (Fig. 1). However the transition temperature is not greatly increased with increasing pressure. Above 95 GPa the boundary of the reaction hcp + fcc \rightarrow fcc in Fe-5Ni-4Si is placed at a lower temperature than the hcp \rightarrow hcp + fcc boundary in Fe-9.7Ni (Fig. 6). This is even more impor-

Table 2
Clausius–Clapeyron slope of the fcc–hcp transitions.

	Fe ^a	Fe–9.7Ni ^b	Fe–4Si ^c	Fe–5Ni–4Si
dP/dT , GPa/K	0.0394	0.0426	0.0394	0.0480
ΔV , cm ³ /mol	0.0679	0.0632	0.0477	0.0377
ΔS , J/K/mol	2.67	2.69	1.88	1.81

^a Komabayashi et al. (2009).

^b Komabayashi et al. (2012).

^c Komabayashi et al. (2019).

tant because Fe–5Ni–4Si contains less Ni than Fe–9.7Ni. As such the simultaneous addition of Ni and Si has an anomalous effect on the transition pressure and temperature, namely greatly stabilising the fcc structure under high pressure.

The above observations indicate that the dP/dT slope of the boundary is significantly increased with the addition of Ni and Si. The dP/dT slopes of the fcc–hcp transition boundaries in different systems and related properties which include the volume change (ΔV) and entropy change (ΔS) at the transition are summarized in Table 2. The dP/dT slopes and ΔV were directly obtained from the experiments while ΔS are calculated through the Clausius–Clapeyron equation $dP/dT = \Delta S/\Delta V$. Table 2 shows that the increased slope in Fe–5Ni–4Si relative to pure Fe is because of a significantly small ΔV . Interestingly, the addition of Ni alone little changes the properties of Fe, but the addition of Si reduces both ΔS and ΔV . The addition of Ni to Fe–Si little changes ΔS , but reduces ΔV , which leads to the increased dP/dT in Fe–5Ni–4Si. As such the thermodynamic properties of the fcc–hcp transition in Fe–5Ni–4Si cannot readily be explained by a combination of the systems Fe–Ni and Fe–Si. The origin of the enlarged fcc stability may lie in the mixing properties of the phases. The nonideal behaviour of each phase will be studied in the future.

4.3. A new phase diagram for Fe–Ni–Si Earth's core

Fig. 7 shows a phase diagram of Fe–5Ni–4Si reporting the fcc–hcp boundaries together with phase relations in pure Fe (Komabayashi, 2014). The Fe phase diagram by Komabayashi (2014) was adopted because it is consistent with both multianvil and DAC works (e.g., Wagle and Steinle-Neumann, 2018) as well as 1 bar data. For comparison, data of melting experiments of Fe by Anzellini et al. (2013) and Jackson et al. (2013) were also plotted. See Komabayashi (2014) for details. In addition, experimental constraints on melting in Fe–5 wt%Ni–10 wt%Si (Fe–5Ni–10Si) under high pressure were shown as the crosses in Fig. 7 (Morard et al., 2011). Since the melting temperature in Fe–Ni–Si is not greatly different from that in Fe up to 50 GPa, we assumed the same melting curve with the fcc structure for Fe–5Ni–4Si. As the melting loop was not resolved in the previous works, we assumed a narrow melting interval, i.e., between solidus and liquidus, and expressed it as a single thick line (Fig. 7).

The triple point where the fcc, hcp, and liquid phases coexist is located at 100 GPa and 3400 K for pure Fe (Komabayashi, 2014). Assuming the Fe melting curve for the fcc phase, the triple point for Fe–5Ni–4Si is located at 145 GPa and 3750 K (160 GPa and 3800 K with Model A EoS). The melting curve of the hcp phase was obtained from the Clausius–Clapeyron relation at the triple point (inset of Fig. 7) with the thermodynamics of fcc melting (Komabayashi, 2014). Thus-obtained phase diagram is consistent with earlier laser-heated DAC experiments in Fe–4.8Ni–4Si (Sakai et al., 2011), supporting the idea that the hcp structure is stable to the inner core conditions.

Ozawa et al. (2016) reported that the eutectic point in the system Fe–Si became close to the Fe end-member with increasing pressure. From laser-heated DAC experiments, they showed the Si content in the eutectic point was less than 1.5 wt% Si at 127 GPa

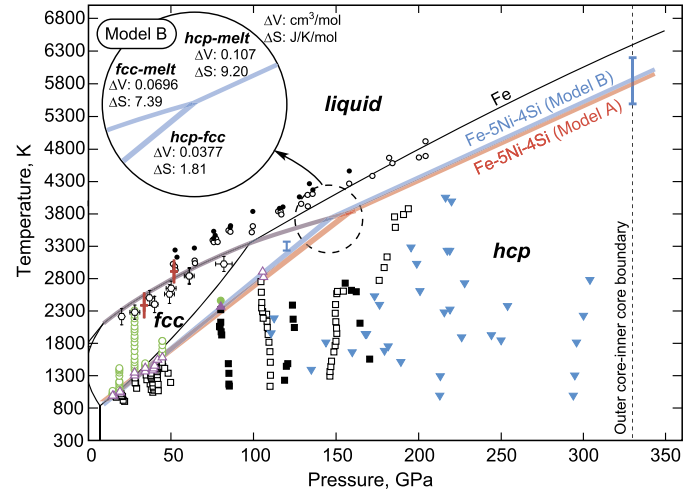


Fig. 7. A new phase diagram for Fe–5Ni–4Si. The present experimental data are plotted together with melting data in Fe (black solid (liquid) and open (crystal) circles, Anzellini et al. (2013); hexagon with error bar, Jackson et al. (2013)) and in Fe–5Ni–10Si (red cross, Morard et al., 2011) and stability of the hcp structure in Fe–4.8Ni–4Si (inverted triangle, Sakai et al. (2011)). Inset: the thermodynamics of the triple point where the hcp, fcc, and liquid phases coexist. The error bars in blue refer to the phase relations with Model B. The error bar on the melting point at 330 GPa was estimated from the following sources. The reaction $hcp + fcc \rightarrow fcc$ may have an uncertainty towards high temperature at pressures greater than the experimental conditions (e.g., 150 K at 120 GPa in the figure). The fcc melting temperatures may have an uncertainty of ± 150 K (Morard et al., 2011). The melting line of the hcp phase might be curved with increasing pressure as is seen in pure Fe, which gives an uncertainty of 200 K towards low temperature at 330 GPa.

Table 3
Physical properties of Fe–5Ni–4Si hcp phase at 330 GPa.

	T (K) ^a	Density (g/cm ³)	K_T ^b (GPa)	α^b ($\times 10^{-5}$ K ⁻¹)	cdd (%)
Model A	5800	12.80	1223	1.20	0.3
Model B	5850	12.84	1294	0.99	0.5

^a The temperature is the melting point in Fig. 7.

^b K_T , isothermal bulk modulus; α , thermal expansion coefficient.

and suggested that the liquidus phase, i.e., a candidate phase for the inner core, would change from the hcp/fcc Fe phase to a CsCl-type phase at about 90 GPa in Fe–4Si. The present experiments show that the phase relations in the system Fe–Ni–Si cannot readily be inferred from the binary systems Fe–Ni and Fe–Si. As such, the direct determination of the liquidus phase in the system Fe–Ni–Si needs to be made in the future.

The melting temperature of the Fe–5Ni–4Si hcp phase at the inner core–outer core boundary (330 GPa) is estimated to be 5850 ± 350 K (5800 ± 350 K with Model A), which is $550 \text{ K} \pm 350 \text{ K}$ lower than pure Fe melting temperature. This is consistent with shock wave measurements in Fe–8 wt%Ni–10 wt%Si (Zhang et al., 2018) although their measurements did not address the structure of the phases. As mentioned above, the melting temperature of Fe–Ni–Si alloy is not very different from that of pure Fe when the alloy structure is fcc (Morard et al., 2011). Due to the shift of the triple point towards high pressure, the melting temperature of hcp alloy should be largely reduced. The melting temperature as well as the melting relations at 330 GPa mentioned above needs to be directly constrained in the system Fe–Ni–Si.

Table 3 lists calculated physical properties of the Fe–5Ni–4Si hcp phase at the inner core–outer core boundary. Both EoS of Models A and B yield a density of the phase close to the inner core density. This means that the cdd can be reconciled with the presence of Si as the sole light element in the inner core. As such, Fig. 7 may be directly applicable for Earth's core.

In conclusion, the present data shed light on the importance of direct determination of the phase relations in the system Fe–Ni–Si for a better understanding of the core properties.

Acknowledgements

We acknowledge DESY (Hamburg, Germany), a member of the Helmholtz Association HGF, for the provision of experimental facilities. Parts of this research were carried out at PETRA III. ESRF (Grenoble, France) is also acknowledged for the provision of experimental facilities at ID27. Both synchrotrons provided financial supports. Two anonymous reviewers are acknowledged for their constructive comments, which improved the quality of the paper. Chris McGuire is thanked for discussions on the XRD patterns. This research was supported by the European Research Council (ERC) Consolidator Grant to TK (Earth core #647723).

Appendix A. Supplementary material

Supplementary material related to this article can be found online at <https://doi.org/10.1016/j.epsl.2019.01.056>.

References

- Alfè, D., Gillan, M.J., Price, G.D., 2002. Composition and temperature of the Earth's core constrained by combining ab initio calculations and seismic data. *Earth Planet. Sci. Lett.* 195, 91–98.
- Allègre, C.J., Poirier, J.P., Humler, E., Hofmann, A.W., 1995. The chemical-composition of the Earth. *Earth Planet. Sci. Lett.* 134, 515–526.
- Antonangeli, D., Komabayashi, T., Occelli, F., Borissenko, E., Walters, A.C., Fiquet, G., Fei, Y.W., 2012. Simultaneous sound velocity and density measurements of hcp iron up to 93 GPa and 1100 K: an experimental test of the Birch's law at high temperature. *Earth Planet. Sci. Lett.* 331, 210–214.
- Antonangeli, D., Siebert, J., Badro, J., Farber, D.L., Fiquet, G., Morard, G., Ryerson, F.J., 2010. Composition of the Earth's inner core from high-pressure sound velocity measurements in Fe–Ni–Si alloys. *Earth Planet. Sci. Lett.* 295, 292–296.
- Anzellini, S., Dewaele, A., Mezouar, M., Loubeyre, P., Morard, G., 2013. Melting of iron at Earth's inner core boundary based on fast X-ray diffraction. *Science* 340, 464–466.
- Asanuma, H., Ohtani, E., Sakai, T., Terasaki, H., Kamada, S., Hirao, N., Sata, N., Ohishi, Y., 2008. Phase relations of Fe–Si alloy up to core conditions: implications for the Earth inner core. *Geophys. Res. Lett.* 35.
- Birch, F., 1952. Elasticity and constitution of the Earth's interior. *J. Geophys. Res.* 57, 227–286.
- Boehler, R., Santamaria-Perez, D., Errandonea, D., Mezouar, M., 2008. Melting, density, and anisotropy of iron at core conditions: new X-ray measurements to 150 GPa. *J. Phys. Conf. Ser.* 121, 022018.
- Dewaele, A., Loubeyre, P., Occelli, F., Mezouar, M., Dorogokupets, P.I., Torrent, M., 2006. Quasihydrostatic equation of state of iron above 2 Mbar. *Phys. Rev. Lett.* 97, 215504.
- Dobson, D.P., Vocadlo, L., Wood, I.G., 2002. A new high-pressure phase of FeSi. *Am. Mineral.* 87, 784–787.
- Fei, Y.W., Murphy, C., Shibasaki, Y., Shahar, A., Huang, H.J., 2016. Thermal equation of state of hcp-iron: constraint on the density deficit of Earth's solid inner core. *Geophys. Res. Lett.* 43, 6837–6843.
- Fischer, R.A., Campbell, A.J., Caracas, R., Reaman, D.M., Heinz, D.L., Dera, P., Prakapenka, V.B., 2014. Equation of state in the Fe–FeSi system at high pressure and temperatures. *J. Geophys. Res.* 119, 2810–2827.
- Fischer, R.A., Campbell, A.J., Reaman, D.M., Miller, N.A., Heinz, D.L., Dera, P., Prakapenka, V.B., 2013. Phase relations in the Fe–FeSi system at high pressures and temperatures. *Earth Planet. Sci. Lett.* 373, 54–64.
- Fitoussi, C., Bourdon, B., Kleine, T., Oberli, F., Reynolds, B.C., 2009. Si isotope systematics of meteorites and terrestrial peridotites: implications for Mg/Si fractionation in the solar nebula and for Si in the Earth's core. *Earth Planet. Sci. Lett.* 287, 77–85.
- Gannarelli, C.M.S., Alfè, D., Gillan, M.J., 2005. The axial ratio of hcp iron at the conditions of the Earth's inner core. *Phys. Earth Planet. Inter.* 152, 67–77.
- Georg, R.B., Halliday, A.N., Schauble, E.A., Reynolds, B.C., 2007. Silicon in the Earth's core. *Nature* 447, 1102–1106. doi:10.1038/nature05927.
- Hammersley, J., 1996. FIT2D V12.012 Reference Manual. Eur. Synchrotron Radiat. Facil., Grenoble, France.
- Hin, R.C., Fitoussi, C., Schmidt, M.W., Bourdon, B., 2014. Experimental determination of the Si isotope fractionation factor between liquid metal and liquid silicate. *Earth Planet. Sci. Lett.* 387, 55–66.
- Jackson, J.M., Sturhahn, W., Lerche, M., Zhao, J.Y., Toellner, T.S., Alp, E.E., Sinogeikin, S.V., Bass, J.D., Murphy, C.A., Wicks, J.K., 2013. Melting of compressed iron by monitoring atomic dynamics. *Earth Planet. Sci. Lett.* 362, 143–150.
- Kamada, S., Suzuki, N., Maeda, F., Hirao, N., Hamada, M., Ohtani, E., Masuda, R., Mitsui, T., Ohishi, Y., Nakano, S., 2018. Electronic properties and compressional behavior of Fe–Si alloys at high pressure. *Am. Mineral.* 103, 1959–1965.
- Kawazoe, T., Ohtani, E., 2006. Reaction between liquid iron and (Mg, Fe)SiO₃-perovskite and solubilities of Si and O in molten iron at 27 GPa. *Phys. Chem. Miner.* 33, 227–234.
- Komabayashi, T., 2014. Thermodynamics of melting relations in the system Fe–FeO at high pressure: implications for oxygen in the Earth's core. *J. Geophys. Res.* 119. <https://doi.org/10.1002/2014JB010980>.
- Komabayashi, T., Fei, Y., Meng, Y., Prakapenka, V., 2009. In-situ X-ray diffraction measurements of the γ - ϵ transition boundary of iron in an internally-heated diamond anvil cell. *Earth Planet. Sci. Lett.* 282, 252–257.
- Komabayashi, T., Hirose, K., Ohishi, Y., 2012. In situ X-ray diffraction measurements of the fcc–hcp phase transition boundary of an Fe–Ni alloy in an internally heated diamond anvil cell. *Phys. Chem. Miner.* 39, 329–338.
- Komabayashi, T., Pesce, G., Morard, G., Antonangeli, D., Sinmyo, R., Mezouar, M., 2019. Phase transition boundary between fcc and hcp structures in Fe–Si alloy and its implications for terrestrial planetary cores. *Am. Mineral.* 104, 94–99. <https://doi.org/10.2138/am-2019-6636>.
- Kuwayama, Y., Hirose, K., 2004. Phase relations in the system Fe–FeSi at 21 GPa. *Am. Mineral.* 89, 273–276.
- Liermann, H.-P., Morgenroth, W., Ehnes, A., Berghäuser, A., Winkler, B., Franz, H., Weckert, E., 2010. The extreme conditions beamline at PETRA III, DESY: possibilities to conduct time resolved monochromatic diffraction experiments in dynamic and laser heated DAC. *J. Phys. Conf. Ser.* 215, 012029. <https://doi.org/10.1088/1742-6596/215/1/012029>.
- Lin, J.F., Heinz, D.L., Campbell, A.J., Devine, J.M., Shen, G.Y., 2002. Iron–silicon alloy in Earth's core? *Science* 295, 313–315.
- Lin, J.F., Scott, H.P., Fischer, R.A., Chang, Y.Y., Kantor, I., Prakapenka, V.B., 2009. Phase relations of Fe–Si alloy in Earth's core. *Geophys. Res. Lett.* 36.
- Litasov, K.D., Sharpygin, I.S., Dorogokupets, P.I., Shatskiy, A., Gavryushkin, P.N., Sokolova, T.S., Ohtani, E., Li, J., Funakoshi, K., 2013. Thermal equation of state and thermodynamic properties of iron carbide Fe₃C to 31 GPa and 1473 K. *J. Geophys. Lett.* 118, 5274–5284.
- Mao, W.L., Campbell, A.J., Heinz, D.L., Shen, G., 2006. Phase relations of Fe–Ni alloys at high pressure and temperature. *Phys. Earth Planet. Inter.* 155, 146–151.
- McDonough, W.F., 2003. Compositional model for the Earth's core. In: *Treatise on Geochemistry*, vol. 2, pp. 547–568.
- Morard, G., Andrault, D., Guignot, N., Siebert, J., Garbarino, G., Antonangeli, D., 2011. Melting of Fe–Ni–Si and Fe–Ni–S alloys at megabar pressures: implications for the core–mantle boundary temperature. *Phys. Chem. Miner.* 38, 767–776.
- Morrison, R.A., Jackson, J.M., Sturhahn, W., Zhang, D., Greenberg, E., 2018. Equations of state and anisotropy of Fe–Ni–Si alloys. *J. Geophys. Res.* 123. doi:10.1029/2017JB015343.
- Ozawa, H., Hirose, K., Yonemitsu, K., Ohishi, Y., 2016. High-pressure melting experiments on Fe–Si alloys and implications for silicon as a light element in the core. *Earth Planet. Sci. Lett.* 456, 47–54.
- Poirier, J.P., 1994. Light-elements in the Earth's outer core – a critical-review. *Phys. Earth Planet. Inter.* 85, 319–337.
- Rubie, D.C., Frost, D.J., Mann, U., Asahara, Y., Nimmo, F., Tsuno, K., Kegler, P., Holzheid, A., Palme, H., 2011. Heterogeneous accretion, composition and core–mantle differentiation of the Earth. *Earth Planet. Sci. Lett.* 301, 31–42.
- Sakai, T., Ohtani, E., Hirao, N., Ohishi, Y., 2011. Stability field of the hcp-structure for Fe, Fe–Ni, and Fe–Ni–Si alloys up to 3 Mbar. *Geophys. Res. Lett.* 38, L09302. doi:10.1029/2010GL047178.
- Shahar, A., Hillgren, V.J., Young, E.D., Fei, Y.W., Macris, C.A., Deng, L.W., 2011. High-temperature Si isotope fractionation between iron metal and silicate. *Geochim. Cosmochim. Acta* 75, 7688–7697.
- Siebert, J., Badro, J., Antonangeli, D., Ryerson, F.J., 2013. Terrestrial accretion under oxidizing conditions. *Science* 339, 1194–1197.
- Tateno, S., Hirose, K., Ohishi, Y., Tatsumi, Y., 2010. The structure of iron in Earth's inner core. *Science* 330, 359–361.
- Tateno, S., Kuwayama, Y., Hirose, K., Ohishi, Y., 2015. The structure of Fe–Si alloy in Earth's inner core. *Earth Planet. Sci. Lett.* 418, 11–19.
- Uchida, T., Wang, Y., Rivers, M.L., Sutton, S.R., 2001. Stability field and thermal equation of state of ϵ -iron determined by synchrotron X-ray diffraction in a multi-anvil apparatus. *J. Geophys. Res.* 106, 21709–21810.
- Wade, J., Wood, B.J., 2005. Core formation and the oxidation state of the Earth. *Earth Planet. Sci. Lett.* 236, 78–95.
- Wagle, F., Steinle-Neumann, G., 2018. Electrical resistivity discontinuity of iron along the melting curve. *Geophys. J. Int.* 213, 237–243.
- Zhang, Y., Sekine, T., Lin, J.-F., He, H., Liu, F., Zhang, M., Sato, T., Zhu, W., Yu, Y., 2018. Shock compression and melting of an Fe–Ni–Si alloy: implications for the temperature profile of the Earth's core and the heat flux across the core–mantle boundary. *J. Geophys. Res.* 123, 1314–1327. <https://doi.org/10.1002/2017JB014723>.